JOURNAL OF GEOPHYSICAL RESEARCH, VOL. 105, NO. B11, PAGES 25,875–25,890, NOVEMBER 10, 2000

Physics of friction and strain rate localization in synthetic fault gouge

Norman H. Sleep
Department of Geophysics, Stanford University, Stanford, California

Eliza Richardson and Chris Marone
Department of Earth, Atmospheric and Planetary Sciences, Massachusetts Institute of Technology, Cambridge

Abstract. Data on synthetic fault gouge previously collected by *Richardson and Marone* [1999] were compared with the predictions of a unified theory for rate- and state-dependent friction compiled by *Sleep* [1997]. The theory treats the gouge as a continuum one-dimensional fluid sheared between parallel plates. It is predicted that the strain rate localized into a shear band of width called W_{ss} during steady state sliding from the nominal width of the gouge zone W_{nom}. The critical displacement during velocity stepping tests is predicted to be $W_{ss}\,\varepsilon_{\text{int}}$, where ε_{int} is the critical strain, an intrinsic material property. It is predicted that the strain rate for renewed sliding after holds delocalizes to a width W_{new} which is greater than W_{ss} and for long holds approaches the full gouge zone width W_{nom}. The displacement for recovery of the shear traction to its steady state value is predicted to be $W_{\text{new}}\varepsilon_{\text{int}}$, which for long holds is much greater than the critical displacement obtained by velocity stepping. Only the macroscopic effects of this process could be studied using the laboratory data in hand. Compaction during the hold and the difference between peak shear traction upon restart and the steady state shear traction during sliding (healing) were measured. To simulate more complex normal traction variations on real faults, the normal traction was varied sinusoidally about its previous value during some holds. The theory reasonably predicts the observed relationship between healing and compaction and healing versus hold time. It predicts the slip needed for recovery of shear traction following holds but poorly predicts the shear traction versus time during recovery. We attribute this failure to the fact that the laboratory gouge is a heterogeneous three-dimensional substance. Qualitatively, the delocalized width W_{new} varies with position within the gouge plane, and slip is required for localized shear to organize in three dimensions. As strain rate was not observed as a function or time and position within the gouge, other explanations for the observed long recovery times following holds remain viable, including consolidation strengthening.

1. Introduction

Experiments on synthetic fault gouge usually measure deformation of thick layers of weak material sandwiched between two or more rigid planar surfaces. Examination of the deformed gouge after an experiment often reveals that strain has localized into a narrow zone within the gouge. Such strain localization affects the frictional properties of the gouge and complicates determination of grain-scale laboratory properties in addition to raising a potential complication in predicting the behavior of gouge within real fault zones.

In this paper, we examine the effect of strain localization on the experimental results of *Richardson and Marone* [1999]. The aftermath of strain localization is evident upon examination of gouge after sliding (Figure 1). The synthetic zone is complicated with oblique (Riedel) shear and intact augen. High-strain shear bands are recognized mainly by the comminution of grains which is an irreversible process on the laboratory time scale. That is, the fine-grain shear bands persist even if the sample is held at rest for a long time after sliding stops.

Paper number 2000JB900288.
0148-0227/00/2000JB900288$09.00

The *Richardson and Marone* [1999] experiments included velocity stepping at constant normal traction, normal traction fluctuations at constant velocity, and normal traction fluctuations during holds. These fluctuations represent special cases of more complicated situations which are expected to occur in Earth. That is, real fault zones experience velocity and normal traction changes during preseismic creep and rupture and normal and shear traction changes from seismic waves and static displacements related to fault movements elsewhere while at rest.

A self-consistent set of relationships which represent the behavior of fault gouge is more useful to earthquake dynamics than a set of epicyclic laws which purport to represent several special cases. Ideally, the theory should be obtainable from considerations of atomistic deformation and equivalent material theory for the lattice of the grains in the gouge. In this paper, we do not attempt a theory with this level of sophistication, but rather we treat the fault gouge as a continuum fluid which in the laboratory is deformed between two rigid plates. We apply the unified rate and state friction theory of *Sleep* [1997], which explicitly includes strain rate localization and normal traction changes. This theory is partly grounded on atomistic and lattice considerations and partly compiled to unify previous empirical relationships. We do not consider alternative theories in detail because none have yet been formulated in enough detail to

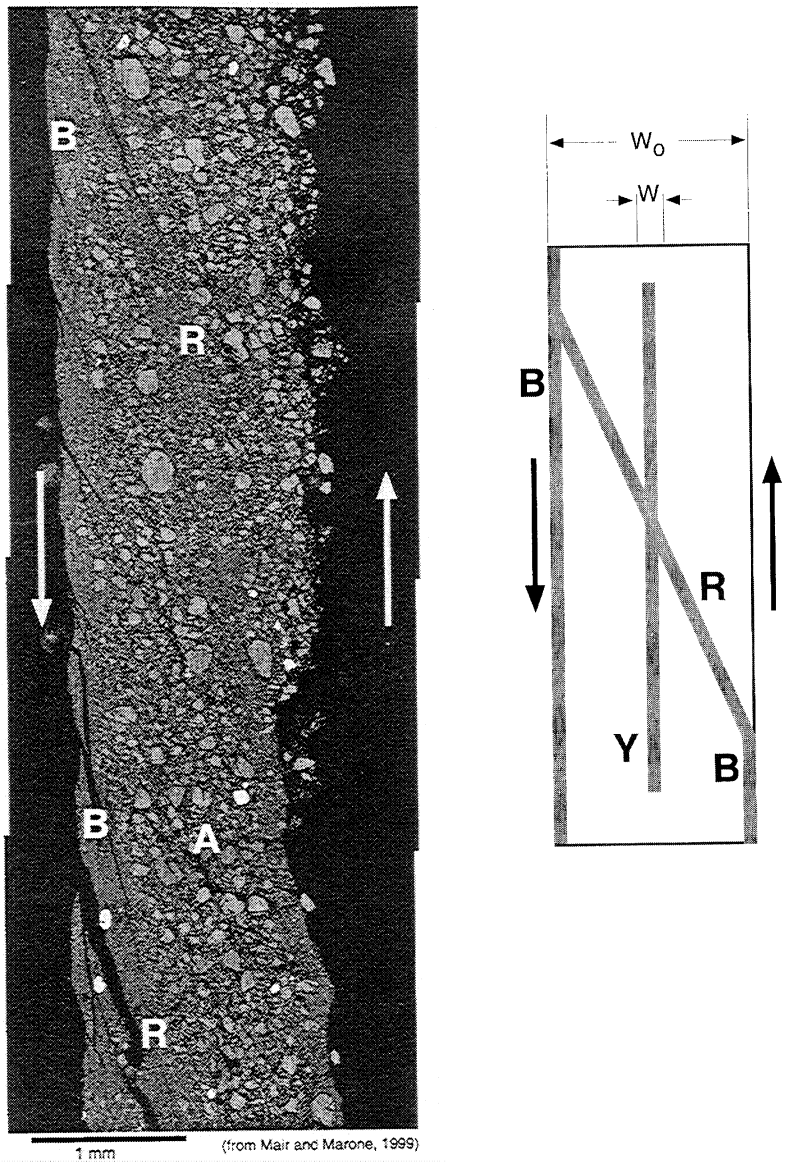

Figure 1. (left) Photomicrograph of a gouge layer showing shear localization and microstructures. B represents boundary shear, R represents Riedel shear, and A denotes an inactive region. Note intense particle size reduction within shear bands. The bright grains are iron oxide present in the starting material. The black open cracks on the left and the ragged edge on the right are effects of sample handling after sliding had finished. (right) Idealized gouge layer of width W_{nom}. In our simple model, strain rate is localized on a Y or B shear of thickness W.

explicitly represent strain rate localization. We show where the theory by *Sleep* [1997] explains experimental observations and where it needs improvement. We use these results to suggest additional laboratory experiments as well as modifications in existing experimental procedures. We make new calculations based on the theory but do not modify it.

2. One-Dimensional Strain Rate Theory

The experimental gouge in Figure 1 is obviously quite complicated. A fully three-dimensional model with tensor stress and strain rate as well as slightly deformable confining walls could be used to represent it. Tensor rate and state friction is discussed by *Sleep* [1998], and deformation associated with the extrusion of laboratory gouge from the contact area is discussed by *Sleep* [1999a]. We take the simpler approach of representing the experimental gouge as one-dimensional flow between two rigid parallel plates. The intrinsic properties of the gouge are assumed to be independent of position within the gouge and of time (or equivalently displacement). Extrinsic properties (for example, strain rate) are assumed to be functions only of the distance x measured perpendicular to the plane of the gouge (Figure 2). This dependence is made explicit in all equations which represent a continuum. One advantage of a one-dimensional model is that simple relationships are not obscured by a complex model.

A second advantage relates to what was actually measured in the *Richardson and Marone* [1999] experiments. The measured shear traction τ and change in gouge layer thickness were macroscopic averages over the contact area of the wall bounding the gouge. The macroscopic variables velocity V and normal traction P (ΔP in the work of *Sleep* [1997]) were controlled.

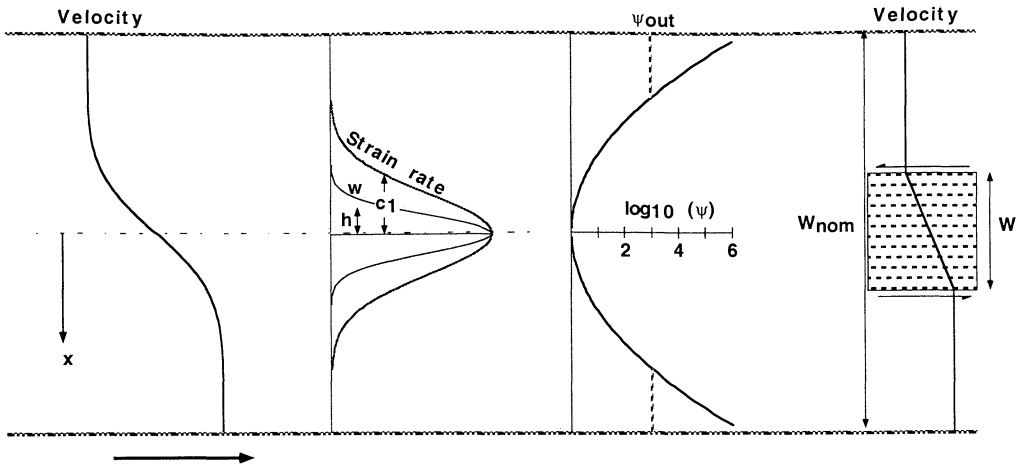

Figure 2. (left) Velocity of a point within the gouge which depends on the position x relative to the center of a high-strain rate zone. Bottom of the gouge zone is sliding to the right. The strain rate can in principle be measured from the derivative of velocity with respect to x. (left middle) Implications of our continuum model for strain rate localization shown schematically. Functions of the distance x into the gouge zone are plotted. The weighting function w has scale width h which is less than the scale width c_1 of the strain rate function. (right middle) Steady state logarithm of the state variable as a parabola. However, the larger values outside of the high strain rate zone cannot be reached during the finite time of the experiment. Rather the state variable outside the high strain zone is ψ_{out}, which increases linearly with time. (right) Shear band represented as a zone of uniform strain rate of width W within a gouge zone of width W_{nom} in the simple model of strain rate localization.

The one-dimensional treatment assumes that shear traction and normal traction are everywhere their macroscopic values. This precludes studying normal traction and gouge pressure variation associated with extrusion of gouge from the fault zone. We represent strain rate within the gouge as simple shear which is spatially uniform within the fault plane, that is, ideal Y shears. This precludes consideration of oblique (Riedel) shears as are often observed in laboratory gouge [*Marone et al.*, 1992; *Gu and Wong*, 1994; *Scott et al.*, 1994; *Nakatani*, 1998; *Mair and Marone*, 1999] and are shown in Figure 1. We return to complications arising from the three-dimensional geometry of the real gouge in sections 3 and 4.

As we wish to model transient changes in friction, we use the strain rate and its localization as kinematic parameters rather than strain. In principle, the strain rate could be measured from the dependence of sliding velocity on position within the fault zone (Figure 2). The strain is measured on a sample after an experiment as in Figure 1.

We alternate between two ways of representing strain rate localization. First, we assume that strain rate is localized within a thickness W of a gouge zone of nominal width W_{nom} (Figure 1). This allows for quick estimation of effects of mature strain rate localization. To study the time-dependent evolution of strain rate localization, we apply a continuum theory previously developed by *Sleep* [1997], which we summarize below.

2.1. Rate and State Friction

Richardson and Marone [1999] interpreted their results in terms of rate and state friction where the strength of the faults depends both on the current rate of slip and on the previous slip history. Because we wish to consider strain rate localization, we follow the notation of *Sleep* [1997], which uses strain and strain rate rather than the macroscopic variables: displacement and velocity. The more traditional macroscopic approach used by *Richardson and Marone* [1999] is recovered when strain rate and strain are assumed to be spatially uniform across the gouge zone.

2.1.1. Macroscopic and local variables. We show both the traditional macroscopic formula and the equivalent local formula for friction and evolution using the notation of *Sleep* [1997] with minor modifications. In terms of macroscopic variables the shear traction is given by

$$\tau = P\,[\mu_0 + a \ln(V/V_0) + b \ln(\psi/\psi_{norm})] \quad , \qquad (1a)$$

where μ_0 is the steady state coefficient of friction, V is the sliding velocity, V_0 is a reference velocity, and a and b are small dimensionless constants. The parameter ψ_{norm} (ψ_0 in the work of *Sleep* [1997]) is a normalizing value of the state variable which (as discussed below) represents the effects of sudden changes in normal traction [*Linker and Dieterich*, 1992] on friction. In terms of the strain rate the friction equation is then

$$\tau = P\,[\mu_0 + a \ln(\dot{\varepsilon}(x)/\dot{\varepsilon}_0) + b \ln(\psi(x)/\psi_{norm})] \quad , \qquad (1b)$$

where strain rate (when it is spatially uniform) is $\dot{\varepsilon} \equiv V/W_{nom}$ and the reference strain rate $\dot{\varepsilon}_0$ is V_0/W_{nom}, where W_{nom} is the nominal width of the gouge zone.

To represent time-dependent behavior of real and simulated fault zones, it is necessary to explicitly relate the state variable ψ to slip history. A variety of equations have been used to do this. We use an interpretation of the "slowness" equation (also referred to as Dieterich's law) in terms of porosity and material properties compiled by *Sleep* [1997]. The evolution equation for the state variable in normalized form using macroscopic variables at isothermal conditions is

$$\frac{\partial \psi}{\partial t} = \frac{V_0 P^{\alpha/b}}{D_c P_0^{\alpha/b}} - \frac{\psi V}{D_c} \quad , \qquad (2a)$$

where t is time, P_0 is a reference normal traction, and α is a dimensionless parameter obtained from experiments where the normal traction is suddenly changed as a controlled variable

[*Linker and Dieterich*, 1992] (α/b is N in the work of *Sleep* [1998] and n in the work of *Sleep* [1997]). In terms of strains and strain rates the evolution equation is

$$\frac{\partial\psi(x)}{\partial t} = \frac{\dot{\varepsilon}_0(x)P^{\alpha/b}}{\varepsilon_{int}P_0^{\alpha/b}} - \frac{\psi\dot{\varepsilon}(x)}{\varepsilon_{int}} \quad , \tag{2b}$$

where the critical strain to significantly modify the state variable is defined in terms of macroscopic variables as

$$\varepsilon_{int} \equiv \frac{D_c}{W_{nom}} \quad , \tag{3}$$

where D_c is the critical displacement in the case that no strain localization is present. The critical displacement is the amount of slip for renewal of contact junctions between solid surfaces, and equation (3) has been demonstrated experimentally for gouge [*Marone and Kilgore*, 1993]. Here the critical strain is considered to be an intrinsic local material property (which by assumption is not a function of position), while the measured value of the critical displacement $\varepsilon_{int}W_{nom}$ when no strain localization occurs depends on the gouge thickness W_{nom}. (The notation has been modified to ε_{int} from ε_0 of *Sleep* [1997] to highlight the intrinsic nature of this parameter.) The local evolution equation (2b) and the local friction equation (1b) reduce to their macroscopic forms (2a) and (1a) when the strain rate is spatially invariant throughout the gouge.

2.1.2. Normal traction changes. The normalizing parameter ψ_{norm} in (1) and the parameter α in (2) are obtained (respectively) by considering the dependence of steady state and transient friction on normal traction following *Sleep* [1997]. To do this, we note that the observed friction in (1) depends on the ratio ψ/ψ_{norm}. Thus we are free to consistently normalize ψ and ψ_{norm} for our convenience. The normalization in (2b) is selected to have the property that $\psi = 1$ for steady state sliding at the reference strain rate, $\dot{\varepsilon} = \dot{\varepsilon}_0$ and the effective normal traction, $P = P_0$. In general, the steady state value of ψ in (2b) is

$$\psi_{ss} = \frac{P^{\alpha/b}\dot{\varepsilon}_0}{P_0^{\alpha/b}\dot{\varepsilon}} \quad . \tag{4}$$

The parameter ψ_{norm} is obtained in terms of physical quantities by assuming that the steady state value of coefficient of friction τ/P is independent of P. That is, $\psi_{ss}/\psi_{norm} = \dot{\varepsilon}_0/\dot{\varepsilon}$, which yields

$$\psi_{norm} = \frac{P^{\alpha/b}}{P_0^{\alpha/b}} \tag{5}$$

[*Sleep*, 1997]. The parameter α is obtained experimentally by measuring the shear traction after a sudden change in normal traction from steady state sliding at P_{old} to P_{new}. The state variable then has no time to evolve from its previous steady state value in (4) of $P_{old}^{\alpha/b}\dot{\varepsilon}_0/P_0^{\alpha/b}\dot{\varepsilon}$. The normalizing parameter ψ_{norm} in (5) instantaneously changes to $P_{new}^{\alpha/b}/P_0^{\alpha/b}$. The coefficient of friction τ/p in (1b) then instantaneously changes by an amount of $\alpha\ln(P_{old}/P_{new})$. The combination of the macroscopic shear traction equation (1a), the macroscopic evolution equation (2a), and the reference state variable equation (5) yields predictions which are mathematically identical to those of the formulation of *Linker and Dieterich* [1992]. Their formulation has the state variable change suddenly when normal traction changes, while our formulation has ψ_{norm} change suddenly.

2.2. Simple Strain Rate Localization Model

We first consider the effects of mature strain rate localization on velocity stepping, normal traction stepping, and slide-hold tests as done by *Richardson and Marone* [1999]. To obtain closed-form results, strain rate is (by assumption) uniform within a shear band of thickness W in a gouge layer of nominal thickness W_{nom} and zero outside this zone (Figure 1). The nominal strain rate $\dot{\varepsilon}_{nom}$ is thus V/W_{nom}, while the actual strain rate $\dot{\varepsilon}_{act}$ is V/W.

To model this strain rate localization, we express (1b) as a local flow law

$$\dot{\varepsilon}(x) = \dot{\varepsilon}_0\left[\frac{\psi_{norm}}{\psi(x)}\right]^{b/a}\exp\left[\frac{\tau-\mu_0 P}{aP}\right] \quad . \tag{6}$$

Equation (6) explicitly allows the strain rate and the state variable to be functions of position x across the fault plane. The macroscopic velocity V is obtained by integrating $\dot{\varepsilon}$ across the fault plane. We consider the effects of this simple strain rate localization model on some idealized experiments which are commonly conducted in the laboratory,

2.2.1. Velocity stepping experiment. In a velocity stepping experiment the gouge zone is brought to steady state at velocity V_{old} and then the velocity is suddenly changed to velocity V_{new}. Letting the normal traction be the reference $P = P_0$, the actual value of ψ within the shear band at steady state from (4) is

$$\psi_{old} = \frac{\dot{\varepsilon}_0}{\dot{\varepsilon}_{old}} = \frac{W\dot{\varepsilon}_0}{V_{old}} \quad . \tag{7}$$

When the velocity is changed, the new strain rate is $\dot{\varepsilon}_{new} = V_{new}/W$. The instantaneous change in shear traction from (1b) is

$$\Delta\tau = P[a\ln(\dot{\varepsilon}_{new}/\dot{\varepsilon}_{old})] = P[a\ln(V_{new}/V_{old})] \quad , \tag{8}$$

which is independent of strain localization. Similarly, the value of ψ after the fault goes to steady state is

$$\psi_{new} = \frac{\dot{\varepsilon}_0}{\dot{\varepsilon}_{new}} = \frac{W\dot{\varepsilon}_0}{V_{new}} \quad . \tag{9}$$

This implies that the steady state change in shear traction is

$$\Delta\tau = P[(a-b)\ln(\dot{\varepsilon}_{new}/\dot{\varepsilon}_{old})] = P[(a-b)\ln(V_{new}/V_{old})] \quad , \tag{10}$$

which is again independent of strain rate localization. That is, the measured values of a and b are not affected by strain rate localization. This result is true only if the width (here represented by W) of the high-strain rate zone remains unchanged during the experiment.

In an actual velocity stepping experiment the shear traction following the velocity step is measured as a function of time and displacement. By solving the macroscopic evolution equation (2a) with V constant, the state variable exponentially approaches its steady state value over a time D_c/V or a distance D_c. The apparent value of the critical displacement obtained by measuring the scale distance for this exponential decay is affected by strain localization [*Marone and Kilgore*, 1993]. The time for slip of the critical strain ε_{int} to occur at the velocity V_{new} is

$$t = \frac{\varepsilon_{int}}{\dot{\varepsilon}_{new}} = \frac{W\varepsilon_{int}}{V_{new}} \tag{11}$$

where the result applies in general as the time for the state variable to approach steady state at a new strain rate. During this time the gouge slides a distance equal to the apparent value of the critical displacement

$$D_{app} \equiv tV_{new} = W\varepsilon_{int} = \frac{WD_c}{W_{nom}} \quad , \tag{12a}$$

which is less than the value without strain localization by a factor of W/W_{nom}. Equivalently, the apparent value of the critical strain is

$$\varepsilon_{app} = W\varepsilon_{int}/W_{nom} \quad . \tag{12b}$$

The key point of (12a) and (12b) is that D_{app} scales with strain localization width, and the micromechanical connection between D_{app} and the critical distance for particle-particle or asperity contacts [e.g., *Dieterich and Kilgore*, 1994] is made by summing the contribution of interparticle contacts within the shear band.

2.2.2. Dilatancy associated with velocity stepping. The change in porosity after a step increase in velocity may be measured with a fluid volume technique [*Marone and Scholz*, 1989; *Marone et al.*, 1990] or by recording how far the walls of the gouge zone move apart [*Marone et al.*, 1990; *Marone and Kilgore*, 1993]. The results of such experiments were interpreted by *Segall and Rice* [1995] and by *Beeler and Tullis* [1997]. The *Beeler and Tullis* [1997] interpretation involves the effect of the energy that dilates the fault zone on macroscopic friction. As we do not have a useful way to extend it for our present purpose, we follow *Segall and Rice* [1995]. They expressed the state variable as a function of porosity

$$\phi - f \equiv C_\varepsilon \ln(\psi) \quad , \tag{13}$$

where ϕ is a reference porosity at which ψ is 1, f is porosity, and C_ε is an empirical dimensionless constant.

The coefficient C_ε can be measured using the change in steady state porosity before and after the velocity step. The initial porosity, from (13) and (7), is

$$f_{old} = \phi - C_\varepsilon \ln\left[\frac{W\dot{\varepsilon}_0}{V_{old}}\right] \quad , \tag{14}$$

and the new porosity in the shear band, from (9), is

$$f_{new} = \phi - C_\varepsilon \ln\left[\frac{W\dot{\varepsilon}_0}{V_{new}}\right] \quad . \tag{15}$$

The difference is

$$\Delta f = C_\varepsilon \ln\left[\frac{V_{new}}{V_{old}}\right] \quad , \tag{16}$$

which is independent of strain localization.

In double-direct shear experiments, such as those conducted by *Richardson and Marone* [1999], dilatation is in practice measured by the changes in the macroscopic distance between the walls of the fault zone. When the strain rate is localized, this change is $W\Delta f$ (assuming that no deformation occurs outside the shear zone). The apparent value of C_ε is obtained, however, by assuming that dilatation occurred uniformly throughout the nominal width of the gouge zone W_{nom}. The apparent dilation parameter. from (16), is then

$$C_{app} \equiv \frac{\frac{W\Delta f}{W_{nom}}}{\ln\left[\frac{V_{new}}{V_{old}}\right]} = \frac{WC_\varepsilon}{W_{nom}} \quad . \tag{17}$$

From (12b) and (17) we find the ratio

$$\frac{C_{app}}{\varepsilon_{app}} = \frac{C_\varepsilon}{\varepsilon_{int}} \tag{18}$$

is independent of strain localization. The physical significance of this ratio is seen by combining (2b) and (13) to obtain an evolution equation for porosity

$$\frac{\partial f(x)}{\partial t} = \frac{\partial \psi(x)}{\partial t}\frac{\partial f(x)}{\partial \psi(x)} = \frac{C_\varepsilon \dot{\varepsilon}(x)}{\varepsilon_{int}} - \frac{C_\varepsilon \dot{\varepsilon}_0 P^{\alpha/b}}{\psi(x)\varepsilon_{int} P_0^{\alpha/b}} \quad , \tag{19}$$

where the first term represents frictional dilatancy and the second represents ductile compaction. The physical significance of the ratio $C_\varepsilon/\varepsilon_{int}$ in (18) is obtained by noting that it multiplies $\dot{\varepsilon}$ in the frictional dilatancy term in (19). The ratio $C_\varepsilon/\varepsilon_{int}$ is thus the ratio of the frictional dilatational strain rate (part of

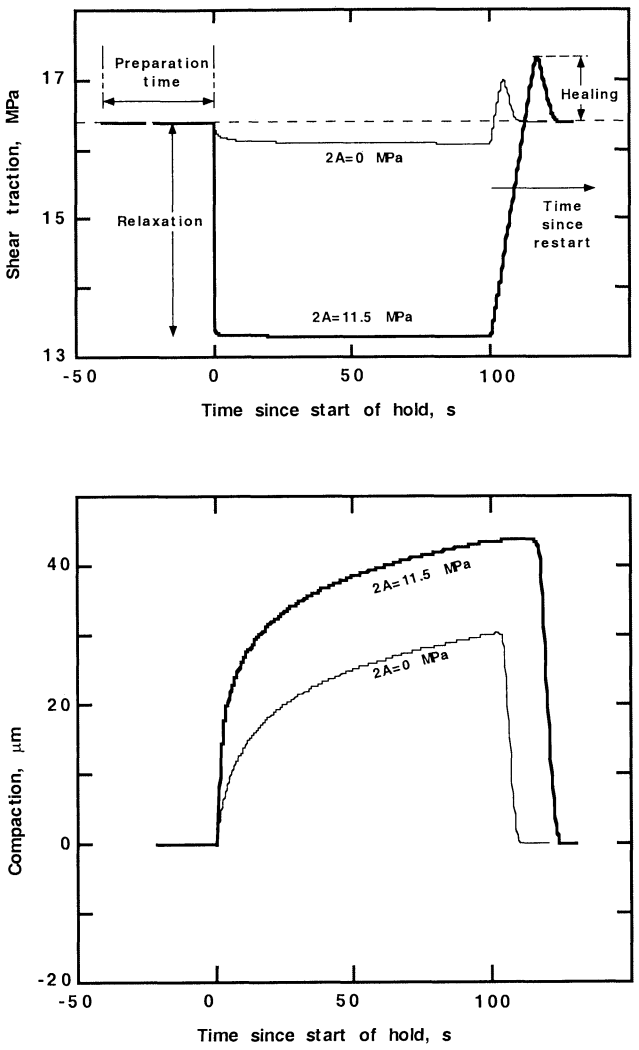

Figure 3. Results of a numerical experiment where it is assumed that the strain rate is uniform within the gouge zone used to illustrate what is measured in a typical slide-hold experiment. After a preparation time to bring the sample to steady state, the load point is stopped. (In this special case, the preparation time has no effect on the results and is shown schematically.) The decrease in shear traction during the hold from continued slip on the gouge is called relaxation (above). The peak shear traction above its previous value is called healing. The recovery of shear traction may be measured as a function of time from restart (top) or alternatively as a function of time from that of the peak shear traction (not shown). Compaction during the hold is shown (below). The stiffness is 25 MPa mm^{-1}. The normal traction is assumed to be sinusoidally oscillated about its previous value with a full amplitude of $2A$ during the hold.

$\partial f/\partial t$) to shear strain rate $\dot{\varepsilon}$. *Sleep* [1997] assumed that this ratio was an intrinsic material constant to derive (19).

2.2.3. Slide-hold tests. In a slide-hold test, sliding is stopped for a period of time and then restarted at its previous velocity and normal traction. Normal traction may be varied during the hold. Compaction during the hold and shear traction upon and after restart are measured. Slight amounts of slip occur during the hold because of finite apparatus stiffness [*Richardson and Marone*, 1999]. We first consider an ideal hold where no slip occurs.

The behavior of the gouge region outside of the high-strain shear band must be explicitly considered to represent a slide-hold test. The experiments of *Richardson and Marone* [1999] were started with preground gouge. The initial slip in the gouge was not localized, and some strain occurred throughout the gouge before the strain rate localized. The evolution of the state variable outside the high-strain rate zone can be inferred from (2b). At the constant normal traction conditions during sliding in the experiments the state variable outside of the high strain zone increases linearly with time. Its value remains finite over the finite preparation time of the experiments. At the start of a hold its value is unknown; we call it ψ_{out}. Note that the preparation time must be distinguished from the hold time and the time since restart from a hold (Figure 3). In general, the evolution equation (2b) for regions outside the shear band where the strain rate is zero is

$$\frac{\partial \psi(x)}{\partial t} = \frac{\dot{\varepsilon}_0 P^{\alpha/b}}{\varepsilon_{int} P_0^{\alpha/b}} \quad . \tag{20}$$

This equation applies throughout the entire gouge layer during holds.

We consider a hold where the previous normal traction is the reference value P_0 without loss of generality. The initial value of ψ_{old} in the shear band is given by (7). Once the hold starts, ψ both within and outside of shear bands increases by the same amount in (20). That is, the changes in ψ and the delocalization associated with them are not instantaneous within the theoretical framework but depend on hold time.

Conditions for strain rate delocalization upon restart are obtained from (6). For simplicity, the strain rate within the shear band prior to the start of the hold is assumed to be the steady state value ψ_{old} in (7) and the width of the shear band is assumed to be its steady state value which we call W_{ss}. The ratio of strain rate inside the previous high-strain zone to the strain rate outside in the rest of the gouge upon restart depends on the ratio of ψ outside to ψ inside to the power of b/a. That is, strain remains localized within a shear band of given thickness when the ratio $(\psi_{old}+I)/(\psi_{out}+I)$ is small, where the change of ψ over time is

$$I \equiv \int \frac{\dot{\varepsilon}_0 P^{\alpha/b}}{\varepsilon_{int} P_0^{\alpha/b}}\, dt \quad . \tag{21}$$

Both the short- and long-term limits of the ratio yield simple expressions.

In the short time limit, I is much smaller than ψ_{out}, and strain rate remains localized. (Conditions for the limit can be obtained by evaluating I.) The strain rate upon restart is hence the previous strain rate and the change in shear traction from the steady state value is from (20)

$$\Delta\tau = P_0 b \, \ln\left[\frac{\psi_{old}+I}{\psi_{old}}\right] \quad . \tag{22}$$

The change in porosity from (13) is

$$\Delta f = -C_\varepsilon \ln\left[\frac{\psi_{old}+I}{\psi_{old}}\right] \quad . \tag{23}$$

In terms of the observable macroscopic quantities the ratio of the change in compaction to the changes in shear traction is

$$-\frac{\Delta f W_{ss}}{\Delta\tau} = \frac{C_\varepsilon W_{ss}}{P_0 b} \quad , \tag{24}$$

which implies that the apparent ratio of C_ε/b is W_{ss}/W_{nom} of the actual ratio.

For long hold times where $I \gg \psi_{out}$, there is little strain localization on restart in the theoretical model. The initial high strain zone can be ignored for computing shear traction. The new (uniform) strain rate throughout the full nominal thickness W_{nom} is W_{ss}/W_{nom} of the previous steady state one. The change in shear traction upon restart is

$$\Delta\tau = P_0\left[a \ln\left(\frac{W_{ss}}{W_{nom}}\right) + b \ln\left(\frac{\psi_{out}+I}{\psi_{old}}\right)\right] \quad . \tag{25}$$

The change in porosity within the shear band is

$$\Delta f_{in} = -C_\varepsilon \ln\left[\frac{\psi_{old}+I}{\psi_{old}}\right] \quad , \tag{26a}$$

and the change outside the shear band is

$$\Delta f_{out} = -C_\varepsilon \ln\left[\frac{\psi_{out}+I}{\psi_{out}}\right] \quad . \tag{26b}$$

In the limit of very long times when I is large, the effect of the preexisting shear band on the numerator of (26a) can be ignored because $\psi_{old} + I \approx \psi_{out} + I$. The compaction is the sum of the changes inside and outside of the shear band:

$$\begin{aligned} -W_{nom}\Delta f_{app} &= -W_{ss}\Delta f_{in} - (W_{nom}-W_{ss})\Delta f_{out} \\ &\approx W_{ss} C_\varepsilon \ln\left[\frac{\psi_{out}}{\psi_{old}}\right] + W_{nom} C_\varepsilon \ln\left[\frac{\psi_{out}+I}{\psi_{out}}\right] \quad , \end{aligned} \tag{27}$$

where Δf_{app} is the average value of porosity change through the gouge zone.

Again returning to macroscopic variables, the rate of change of shear traction relative to compaction from (25) and (27) is

$$-W_{nom}\frac{\partial \Delta f_{app}}{\partial \tau} = \frac{C_\varepsilon W_{nom}}{P_0 b} \quad . \tag{28}$$

This limiting slope is predicted to be independent of the history of the sample, including that prior to the start of the hold and of the steady state width of the shear band W_{ss}.

To reiterate, the results of a slide hold test may be plotted as the degree of compaction of the fault zone versus the increase in shear traction from its previous steady state value upon restart (Figure 4). At short times the curve is linear with a slope of $W_{ss} C_\varepsilon/bP_0$ and passes through the origin. At long times the slope is $W_{nom} C_\varepsilon/bP_0$, but the curve does not pass through the origin. In principle, the amount of strain localization is given by the ratio of the slopes at large and small times. The long time slope is the same slope that would occur in the absence of any strain localization (which can be seen by setting $W_{ss} = W_{nom}$ in (24) or in (25) and (26)). In the case starting with uniform strain rate in the gouge, the curve goes directly through the origin. In both cases, the value of C_ε can be determined from (28)

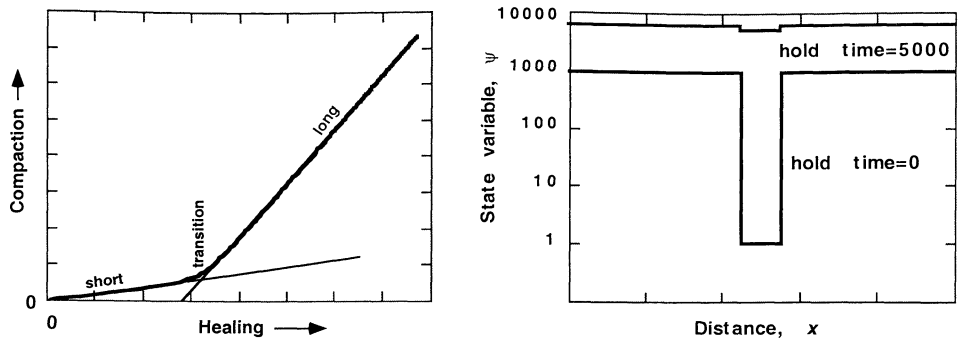

Figure 4. (left) Relationship between healing and compaction for the simple model of a shear band of width W within a gouge zone of width W_{nom} shown schematically. At short times, behavior is controlled by the localized shear band and at long times it is controlled by the full width of the gouge zone. The extrapolations of the linear segments of the curves are shown by thin lines. Here it is assumed that the high-strain rate zone is 0.1 of the gouge zone thickness and that a value of ψ within the high-strain rate zone is 1 at the start of the hold compared to $\psi = 1000$ outside. (right) State variable plotted as a function of position x within the gouge zone (right) at the start of the hold and after passage of a hold time which increases the state variable everywhere by 5000. The ratio of the state variable inside the shear band to that outside approaches 1 in the limit of long hold times. The position of the shear band within the gouge zone is arbitrary and does not effect the predictions of this simple model.

and from data taken at long times where the entire gouge zone is compacting.

In addition, the parameters b and C_{app} are measured independently on velocity stepping tests. The localized width W and the nominal width W_{nom} of the gouge zone can be measured independently if one is able to solve the very difficult problem of imaging the interior of a sample during sliding.

The plot in Figure 4 of compaction versus frictional healing (peak increase of shear traction above its previous steady state value after restart in Figure 3) is independent of the exponent α/b and the history of normal traction during the hold. This can be seen from (22), (23), (25), and (26). The normal traction history and α/b appear only through (21) in the integral I. That is, the value of I, not the path by which it was reached, affects this plot. We take advantage of these features when addressing real data in sections 3.2. and 3.3.

2.3. Numerical Strain Localization Model

The analytical results in the previous section are useful for understanding the qualitative behavior of fault gouge with strain localization. A more quantitative representation is desirable for comparison with laboratory data. We apply a formalism developed by *Sleep* [1997], which is not rigorously derived but does have the necessary properties of a one-dimensional strain rate localization theory.

2.3.1. Continuum theory. We apply the result of *Sleep* [1997] that strain rate localization during sliding occurs spontaneously provided that $b > a$ in (1b). In this case, the steady state shear traction decreases with increasing strain rate which can be obtained by combining (1b), (4), and (5)

$$\tau_{ss} = P[\mu_0 + (a-b)\ln(\dot{\varepsilon}/\dot{\varepsilon}_0)] \quad . \tag{29}$$

It is evident that a very large strain rate produced by extreme strain rate localization would produce a very low shear traction. This creates a problem when strain rate is represented by a numerical grid. Unless special precautions are taken to prevent it, the strain rate will localize to a single numerical grid or element [e.g., *Delaplace et al.*, 1996]. This makes the final result unacceptably dependent on the grid spacing instead of on physical properties of the gouge such as grain size and shear band width.

Sleep [1997] let the evolution equation for the state variable be in our notation be

$$\frac{\partial\psi(x)}{\partial t} = \frac{\dot{\varepsilon}_0 P^{\alpha/b}}{\varepsilon_{int} P_0^{\alpha/b}} - \frac{\psi[\dot{\varepsilon}(x) * w(x)]}{\varepsilon_{int}} \quad , \tag{30}$$

where the asterisk denotes convolution, x is distance across the gouge zone, and

$$w(x) = w_1 \exp[-x^2/h^2] \tag{31}$$

is a weighting function, where w_1 is a normalizing factor so that the integral of the weighting function from $-\infty$ to ∞ is 1 and h is a length scale (Figure 2). The form of the evolution equation (30) retains the same physics as the simple form (2b), except that the strain rate-dependent term depends on a spatial average.

Equations (29) and (30) along with the flow law in (6) can be solved analytically for steady state sliding. Following *Sleep* [1997], the steady state strain function is

$$\dot{\varepsilon}(x) = \dot{\varepsilon}_1 \exp[-x^2/c_1^2] \quad , \tag{32}$$

where $\dot{\varepsilon}_1$ is a constant and c_1 is the length scale for strain rate localization. The steady state value of the state variable is

$$\psi(x) = \psi_1 \exp[x^2/c_\psi^2] \quad , \tag{33}$$

where ψ_1 is a constant and c_ψ is the length scale for the state variable. Note that ψ is predicted to remain finite (rather than having exponentially large values for large $|x|$) because there is only finite time for evolution in (30) to occur in a real experiment.

Spatial invariance of shear traction across the fault zone implies that $ac_1^2 = bc_\psi^2$, which can be seen most easily by substituting (32) for $\dot{\varepsilon}$ and (33) for ψ into (1b). Solving (30) for steady state conditions by invoking the convolution theorem yields the length scale for strain localization

$$c_1 = h\left[\frac{b}{a} - 1\right]^{-1/2}, \quad (34)$$

which has real-valued solutions only when $b > a$ (Figure 2). That is, the condition for strain localization (mathematically that c_1 is real in (32)) is the same as that for velocity instability with sliding at constant shear traction $b > a$. This formulation has the desired result that the width of strain rate localization is given by physical parameters (h, a, and b), not a numerical grid.

The formulation of the continuum in (30) can be qualitatively understood if $\dot{\varepsilon}(x)$ is a macroscopic value obtained by averaging the actual instantaneous microscopic strain rate over a planar surface a distance x into the gouge zone. The damage (say tail cracks or dilation within a densely packed granular aggregate) from the strain rate at any point in the gouge zone is distributed over a distance h perpendicular to the layer about x because the finite size of grains limits localization. We do not, however, have a way to find h from grain size by first principles. Here h denotes the effective width of a shear band with diffuse boundaries. The weighting function $w(x)$ gives the probability of damage (or frictional dilatancy) occurring around the nominal position x of the shear band. Thus in the sense that $w(x)$ determines where in the shear band the next increment of strain will be accommodated, it is crudely analogous to a wave function in quantum mechanics telling the probability of where a particle might be detected. The Gaussian form in (30) is attractive in that it introduces a characteristic length in a way which appears in numerous cases where probability is involved and yields clean analytical solutions. The form of the strain rate function (here (32)) provides a test of the validity of the weighting function w in (31) and the continuum theory in general. Unfortunately, we have no way to directly measure strain rate within the gouge during sliding.

2.3.2. Relationship of continuum and simple models. The results of the simple model in which the shear band is of width W are helpful for qualitatively explaining features that arise from numerical experiments based on the continuum formulation. Qualitatively comparison is aided by noting that the width $2c_1$ is a more sophisticated representation of the shear band width W in the simple model. The effective steady state width W_{ss} of a shear band in the continuum model is proportional to h from c_1 in (34). For the numerical representation to work, the length h must be represented by several grid points; we use 8. The length h also needs to be significantly less then the width of the gouge zone W_{nom}, so that the boundaries of the zone do not strongly affect the convolution in (30). In the case that h is comparable to or larger than the gouge zone width, little localization occurs and the process is adequately represented by assuming uniform strain rate throughout the fault zone. That is, by using the traditional macroscopic variables velocity and shear traction.

2.3.3. Numerical method. An explicit computational method was used in the numerical models. The state variable $\psi(x)$ and the strain rate $\dot{\varepsilon}$ were represented on node points. Integrals over space were evaluated by summing of the node points.

In several of the models it was assumed that the apparatus was infinitely stiff and the velocity on the walls of the gouge and the normal traction were imposed as boundary conditions. Time steps were done by evaluating (30) to get a new $\psi(x)$ from the old $\psi(x)$ and the old $\dot{\varepsilon}(x)$. A new value of the strain rate $\dot{\varepsilon}(x)$ was obtained from the updated $\psi(x)$ using (6) and solving for τ to have $\dot{\varepsilon}(x)$ integrate to the velocity V across the fault zone. The compaction was obtained from the state variable using (13) and integrating the change in porosity across the fault zone. During holds the strain rate was set to zero in (30), and the healing upon restart was obtained from (6) for the sliding velocity at each time step. Note that the shear traction during the hold from (1b) is undefined for the infinitely stiff apparatus because the strain rate is zero. This feature, however, does not affect evaluation of the evolution equation (30).

Models representing an elastic apparatus differed in that a velocity was imposed at a load point connected to the gouge wall by a spring. A new strain rate $\dot{\varepsilon}(x)$ was obtained from $\psi(x)$ and the shear traction τ using (6). An updated state function $\psi(x)$ was obtained from the old $\psi(x)$ and the new $\dot{\varepsilon}(x)$ using (30). The velocity across the fault zone was obtained by integrating $\dot{\varepsilon}(x)$. The displacement of the wall relatively to the load point during the time step was used to obtain a new value of the shear traction τ on a spring. The procedure gives well-defined shear traction τ during holds as well as at other times.

The results of a numerical experiment in which by assumption no strain rate localization occurs are shown in Figure 3 to illustrate our terminology and for later comparison with models representing strain rate localization. After a preparation time of sliding at constant velocity, a hold is begun. Some slip continues on the gouge plane causing the shear traction to decrease which we call relaxation. When sliding at the load point is restarted, time is required for elastic loading. The difference between the peak shear traction and its previous value is called healing. After a short time, the shear traction returns to its previous steady state value. Compaction occurs during the hold, and the porosity returns to its previous steady state value after some sliding. In this case that there is by assumption no strain rate localization, the results of the numerical experiment are independent of the preparation time because $W = W_{\text{nom}}$, and thus there is no low-strain rate part of the gouge to compact and evolve.

The history of shear traction and compaction was also computed for a model where the normal traction oscillated with $2A = 11.5$ MPA, an amount in some of laboratory experiments by *Richardson and Marone* [1999] (Figure 3). The shear traction relaxes more during the hold than it does for $2A = 0$ becauses some slip occurs when normal traction is low during an oscillation. From (21), compaction and evolution of the state variable occur mainly when the normal traction is high. In this case which does not have strain rate localization, the time for the shear traction to recover to steady state does not strongly depend on the normal traction oscillation $2A$ during the hold or the duration of the hold, but only on the macroscopic critical displacement D_c.

In contrast, the simple theory for strain rate localization indicates that recovery time depends both on preparation time and the "duration" of the hold measured by the integral I in (21). For long preparation times and short holds the strain rate is still localized within the previous high-strain rate zone of width W upon restart. The small amount of slip needed for recovery scales with the apparent critical displacement in (12a). Conversely, the strain rate is delocalization throughout the gouge zone for short preparation times and long holds. The large amount of slip needed for recovery scales with the critical displacement D_c, when strain rate is localized prior to a hold and delocalized after a hold.

3. Comparison of Experiments With Theory

In section 2 the theory developed by *Sleep* [1997] was applied to obtain predicted behavior of gouge during velocity-stepping and slide-hold tests. We compare this theory with experimental results in sections 3.2 and 3.3. Before doing this, we summarize the experimental procedure and how it differed from more idealized computer representations.

3.1. Experimental Procedure

We briefly review the experimental procedure of *Richardson and Marone* [1999]. They used a servocontrolled double-direct shear apparatus. At the start 10 cm×10 cm blocks were separated by 3-mm-thick synthetic gouge layers made of fine-grained 50-150 μm quartz powder. The normal traction and velocity at a load point were controlled. Compaction was measured by the approach of the blocks, and the shear traction was measured at the load point. Two gouge layers were present in the experiments. The total compaction of both layers was measured and the result divided by 2; the average of the shear tractions on the layers was similarly obtained.

Sliding was allowed to progress to allow the gouge to mature. A series of velocity-stepping, normal-traction-stepping, and slide-hold tests were then performed. During some of the holds the normal traction was oscillated sinusoidally about its previous value with a 1-Hz frequency. The purpose of the oscillations is to represent more complicated changes in normal traction that occur on real faults at rest in a simple way. The velocity-stepping experiments constrain rate and state friction parameters independently of the slide-hold tests.

3.1.1. Dependence on starting conditions. The experiments of *Richardson and Marone* [1999] were not planned with the theory of *Sleep* [1997] in mind. Problems in applying the theory arise from its dependence on the starting conditions, which were not well controlled in the experiments.

The numerical slide-hold experiments were started in a way that might be potentially controlled in the laboratory. The numerical experiments are started with essentially delocalized sliding rather than fully delocalized sliding. Perfectly delocalized sliding, which is numerically started using uniform steady state value for $\psi(x)$ in (4), is unacceptable. The state variable in (2b) can never evolve from its initial value because the strain rate is everywhere exactly the uniform macroscopic value. Rather, the starting function $\psi(x)$ needs to be perturbed by subtracting a small amount, $\Delta\psi(x)$, from its uniform steady state value. (An analogous example is a pencil perfectly balanced on its point; it stays put in a computer model but falls if slightly perturbed.) The function $\psi(x)$ then evolves by (2c) with sliding at a constant velocity. Our perturbation function, $\Delta\psi(x)$, has zero mean. The greatest values of $\Delta\psi(x)$ were imposed near the center of the gouge (so that a Y shear and not a B shear resulted), and perturbation function was not exactly symmetric about the center of the gouge (to avoid the special case of symmetric localization). The same arbitrary perturbation was used for all runs at a given h. The position of localization within synthetic gouge is expected by the theory to depend on perturbations from heterogeneities as seen in Figure 1 and not be predictable.

To represent slide hold tests, numerical sliding at constant velocity was maintained for a period of time, and then the hold commenced. The variation of the state variable and the strain rate across the fault zone before the start of the hold are deterministic results of the initial perturbation and the material properties. Basically, a high-strain rate zone formed within the gouge surrounded by an essentially nondeforming region as predicted by both the simple and the continuum models. In the simple model the value of the state variable outside of the high-strain rate zone is (ψ_{out}) at the start of the hold. In numerical simulations the state variable and the strain rate approach their analytical steady state values (given by (33) and (32)) within the zone of significant strain rate. Outside this high-strain rate zone, the strain rate is essentially zero. The second term in the evolution equation (30) is thus essentially zero there. At constant normal traction as occurred during sliding in the laboratory experiments, the state variable outside the high-strain zone increases linearly with time. Its value at the start of the hold (ψ_{out} in the simple model) is approximately the sum of the steady state value in (4) for uniformly distributed shear strain and a term from (21) that is linearly proportional to the preparation time. We use both concepts of ψ_{out} and preparation time to qualitatively discuss our numerical results and the laboratory experiments.

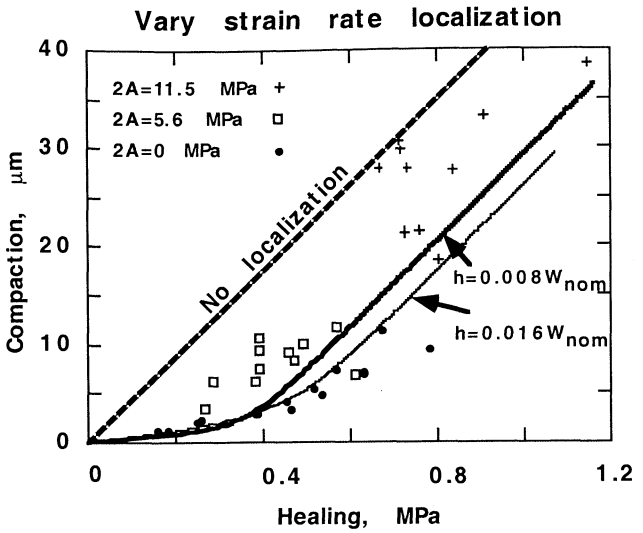

Figure 5. Change of shear traction from its previous steady state value on restart (healing) plotted against compaction during the hold. Experimental results for various normal traction oscillations 2*A* are shown as points. Each point represents a single slide-hold test. The computed curves with strain localization give tolerable fits. The computed curve without strain localization gives a poor fit. All the curves become parallel for large compactions and healings. The computed compaction scales linearly with C_ε and healing scales linearly with b. The preparation time for the theoretical curves is assumed to be 384 s.

Slide-hold testing of *Richardson and Marone* [1999] commenced after the initial properties of the gouge had evolved so that velocity-stepping experiments indicated that $b > a$. Strain rate localization is then theoretically expected from (34). A new hold was started as soon as the shear traction approached a steady state. This allowed many tests to be conducted on each sample but caused the displacement and normal traction history prior to each test to vary.

A potentially avoidable source of scatter arises from the laboratory starting conditions when all the data are grouped on one plot as in Figure 5. The value of ψ_{out} at the start of a given

test was likely to have been somewhat different from the others. We return to the systematic effects of this situation in section 3.3.2.

An unavoidable result of the laboratory procedure is illustrated by Figure 5 where compaction is plotted as a function of healing. Compaction during each hold was measured in the laboratory as a function of time and the compaction at the end of the hold plotted. However, finite slip is needed to measure healing in the laboratory, as illustrated by the numerical simulation in Figure 3. That is, healing could not be measured without ending a hold. The results of a given slide-hold test thus appear as a point on Figure 5. In contrast, the theoretical curve is continuous as it is easy to compute healing that would occur if the sliding was started at a time and to also continue to follow changes in the state variable which would occur if the hold was continued.

3.1.2. Problems with gouge geometry. A minor source of scatter when the data are plotted together (shown in Figure 5) arises because the thickness of the laboratory gouge zone varied from its nominal, initial thickness due to comminution and geometric thinning with slip [*Scott et al.*, 1994]. The magnitude of the effects is constrained by the simple model. It is not possible to usefully normalize compaction to gouge zone thickness W_{nom} for all lengths of holds. For short holds the predicted slope on Figure 5 depends only on the properties of the high-strain rate zone in (24). For very long holds the entire gouge zone compacts during the hold and deforms when sliding is restarted. The problem arising from plotting the compaction rather than compaction normalized to nominal gouge thickness is illustrated by the simple model. From (28), compaction at long times increases with the actual nominal thickness of the gouge layer W_{nom}. Then, the shear traction in the delocalized zone scales from strain rate in (1b) as $aP\ln(W_a/W_{nom})$, where W_a is the assumed thickness of the gouge zone. In the laboratory experiments, W_{nom} is measured precisely, and its absolute value is known to within ≈100 μm. However, W_{nom} is not a controllable parameter due to changes in particle size distribution, particle comminution, and packing. There is some variation as a function of slip and between experiments. As a point of reference, we note that a factor of 2 error in gouge thickness would produce a minor computed shear traction error of 0.1 MPa for the experimental P = 25 MPa and $a = 0.0054$.

3.2. Calibration of Numerical Experiments

We apply our theory and numerical model to represent the behavior of the laboratory gouge zones in an idealized manner. For many of the simulations we assume a perfectly stiff loading apparatus where the normal traction and velocity are controlled and compaction of the fault zone and the shear traction during sliding are measured. That is, the velocity is instantaneously changed during numerical slide-hold and velocity stepping tests. Calculations with finite stiffness (Figure 3) indicate elasticity is expected to have little effect on these quantities.

We are now ready to compare data with theory. *Richardson and Marone* [1999] used a double-direct shear apparatus to measure the properties of their synthetic gouge. Their velocity-stepping experiments constrain a, b, and the apparent value of critical displacement D_{app}. We assume that these parameters are already known before the start of the slide-hold tests and are the same for every test. We use the laboratory velocity stepping experiments to obtain that $a = 0.0054$ and $b = 0.0066$. We calibrate our other material properties using eyeball fits to the observed data. Velocity-stepping experiments reduce the number of free parameters available for interpreting the slide-hold tests.

To appraise the effect of strain localization, we consider two representative gouge zones. In the one with milder strain rate localization the localization scale h is assumed to be $0.016\,W_{nom}$. In the stronger localization model it was assumed that $h = 0.008\,W_{nom}$. From (34) the characteristic steady state thickness of the high-strain zones ($\approx W_{ss}$) are then $2c_1 = 0.068W_{nom}$ and $2c_1 = 0.034W_{nom}$, respectively. The apparent critical displacements are 0.116 and 0.058 of the displacements for uniform strain over W_{nom}, respectively. That is, W_{ss} is these factors times W_{nom} for the two models.

To express the quantities in dimensional units, we use the observed value in a velocity-stepping test of D_{app} = 15 μm for the apparent critical displacement and the actual value of the nominal gouge zone width is $W_{nom} = 2140$ μm (the value obtained in one experiment). The material property ε_{int} in (12a) in the mild localization model is then $15\,\mu m/(2140\,\mu m * 0.116) = 0.06$. In the strongly localized model it is $15\,\mu m/(2140\,\mu m * 0.058) = 0.12$. The high-strain zone widths $2c_1$ are 146 and 73 μm, respectively, which are similar in magnitude to the measured shear band widths (e.g., Figure 1). An estimate of the magnitude of the intrinsic dilatation faction C_ε of 3.4×10^{-3} is obtained by applying the long-time limit in (28) to our healing versus compaction data in Figure 5 using our measured values for $b = 0.0066$, $W_{nom} = 2140$ μm, and normal traction during sliding of $P_0 = 25$ MPa. The exponent α/b is estimated in section 3.3.3 to be ~16 by comparing the time dependence of healing in slide-hold experiments with and without normal traction oscillations. The experimental velocity at steady state was 10 μm s^{-1}.

3.3. Analysis of Data

A key feature of the slide-hold test by *Richardson and Marone* [1999] is that the normal traction was oscillated sinusoidally during holds with a full amplitude of $2A$. This provides a test of the theory as changes in the state variable within the fault zone during a hold are predicted to depend only on the integral I in (21) and not the normal traction versus time path to obtain its value. We thus compare data and predictions for holds with constant normal traction to those with oscillatory normal traction.

3.3.1. Healing versus compaction. We begin by comparing the observed compaction during each hold with observed healing (Figure 5). The predicted curve does not depend upon the parameter α/b. It is also independent of variations of the normal traction during the hold, including the intentional variations represented by the parameter $2A$ and those owing to instrumental vagaries. This feature allows data with various $2A$ and various hold times to be examined together. In Figure 5 it is obvious that the straight line through the origin (which would be expected if no strain localization occurred) is incompatible with the data, implying a finite characteristic localization length h. The curves for $h = 0.008\,W_{nom}$ and $h = 0.016\,W_{nom}$ give comparably reasonable fits within the scatter of the data. For both curves representing strain localization the preparation time is 384 s. This is a reasonable estimate for the laboratory preparation times, which are not well constrained because a complicated history occurred before each hold.

The differences between the $h = 0.008W_{nom}$ and $h = 0.016W_{nom}$ curves can be understood in terms of the simple

localization model discussed above. That is, the width of the steady state high-strain rate zone W_{ss} is a factor of 2 greater for $h = 0.016W_{nom}$ than for $h = 0.008W_{nom}$. At very small compactions the short time limit in (24) holds implying that compaction is proportional to steady state shear band width W_{ss} and to h. This implies that the $h = 0.016W_{nom}$ curve lies above the $h = 0.008W_{nom}$ curve with twice the slope. (In practice, the initial linear region occurs for holds that are too brief to do in the laboratory experiments.) The slope at large values of compaction and healing for both curves is the same as expected from (28). The modest offset between the two curves for large compactions is related to the different critical strains ε_{int}, but a simple expression quantifying the difference as well as a simple qualitative explanation were not found. In any case, the difference between the two curves cannot be resolved within the scatter of the experimental data.

3.3.2. Effect of preparation time. The $2A = 0$ data are systematically below both the $h = 0.008W_{nom}$ and $h = 0.016W_{nom}$ curves and the $2A > 0$ data (Figure 5). The feature may be an unintended artifact of a systematic correlation of the preparation time with $2A$ in the laboratory experiments. The laboratory slide-hold with $2A = 0$ tests were conducted sequentially. The simple theory illustrates the expected consequences. As the integral I in (21) for a given length hold is less for $2A = 0$ than for $2A > 0$, the criterion for delocalization that $I > \psi_{out}$ was less likely to be achieved than for $2A > 0$. Thus the $2A = 0$ holds are expected from the theory to be less likely to delocalize strain rate. During a long series of slide-hold tests the state variable outside of the zone of active slip continued to increase throughout both holds and slides. Conversely, delocalization is expected to have occurred after holds with $2A > 0$, resetting ψ_{out} in each cycle and preventing ψ_{out} from growing with repeated cycles, even though they were also conducted sequentially in the laboratory experiments.

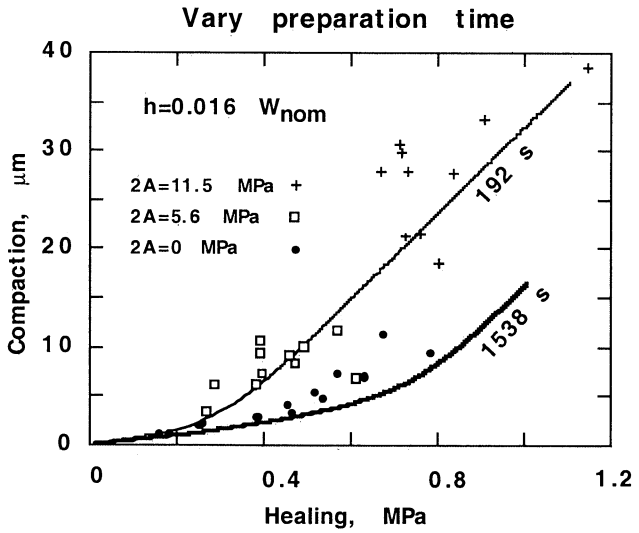

Figure 6. Compaction and healing plotted as in Figure 5. Data are represented by points and theoretical models are represented by curves. The effect of the preparation time since the last strain rate delocalization is shown for $h = 0.016W_{nom}$. The $2A = 0$ data fall between the preparation time of 384 s curve on Figure 5 and the 1538 curve on this figure. These times are within the range applicable to the experiments. Variability in the preparation time is a viable explanation for much of the scatter in the data as well as the systematically low compactions of the $2A = 0$ experiments.

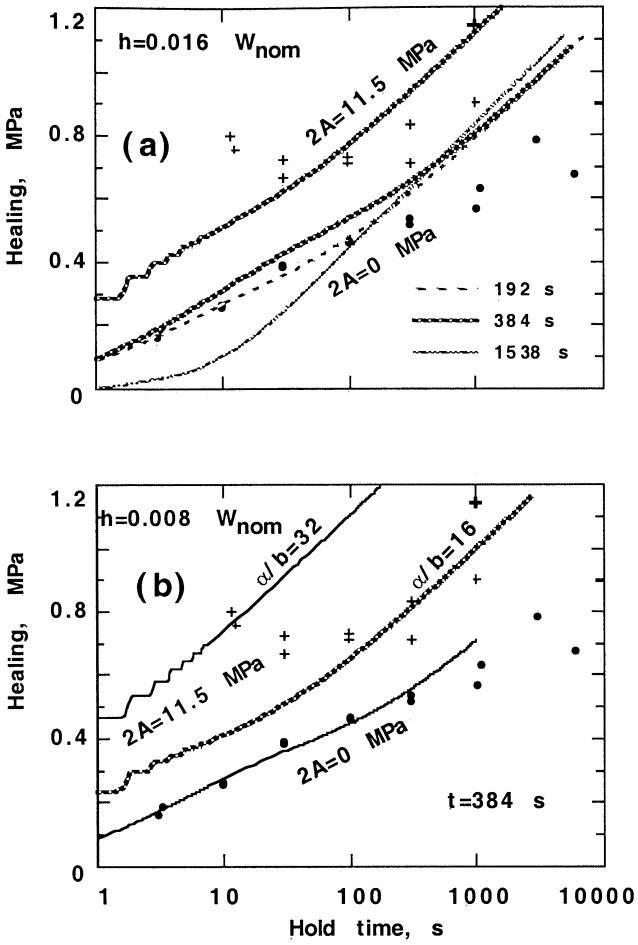

Figure 7. Healing shown as a function of hold time. Experimental data for $2A = 0$ (solid dots) and $2A = 11.5$ MPa (crosses) are shown with numerical results (a) for $h = 0.016W_{nom}$ and (b) for $h = 0.008W_{nom}$. Different lines represent different preparation times since last delocalization for $2A = 0$ (Figure 7a). Healing at longer times is weakly dependent on the preparation time since last strain delocalization (Figure 7a). The $h = 0.008W_{nom}$ model gives a slightly better fit to these scattered data. The difference between the $2A = 0$ and $2A = 11.5$ MPa curves scales with α/b. Curves for $2A = 11.5$ MPa are shown for α/b of 16 and 32 (Figure 7b). All the $2A = 11.5$ MPa curves assume a preparation time of 384 s. Healing scales linearly with b.

The significant theoretical effect of the preparation time on a compaction versus healing plot is shown in Figure 6. In terms of the simple model the criterion for the long time limit in (28) for a linear healing versus compaction curves is that $I \gg \psi_{out}$. The increase in I needed for this is thus greater for long preparation times where ψ_{out} is large. From (25), larger values of I and of ψ_{out} at the point where a curve in Figure 6 becomes linear imply a larger healing at that point. The curve for a preparation time of 192 s goes through the $2A > 0$ points, while a longer preparation time it goes through the $2A = 0$ points. This provides a potential explanation of the difference between the two groups of data. The values of preparation time are reasonable from the experiments but cannot be further quantified

with the available data. This difficulty provides a demonstration that (within the scope of the theory) it is important to control the history before each hold.

3.3.3. Constraining material parameters. The curves of Figures 5 and 6 are independent of the parameter α/b and only weakly dependent on the localization scale h. The variation of healing as a function of hold time constrains of these quantities (Figure 7). Again each laboratory slide-hold test is represented by a point and the numerical solution is represented by continuous curves.

The value of h is constrained by the $2A = 0$ curves which are independent of α/b as normal traction is then constant in (21). The curves are not strongly dependent on the preparation time since the last strain rate delocalization, a parameter which is known to have been poorly controlled in the laboratory experiments. The $h = 0.008\, W_{\text{nom}}$ curves give a slightly better eyeball fit than the $h = 0.016\, W_{\text{nom}}$. (A smaller value of h implies a shallow slope.) This value of $h = 0.008\, W_{\text{nom}}$ is used in the subsequent calculations that model data.

Once the value of h is constrained to be around $0.008\, W_{\text{nom}}$ by the $2A = 0$ curve, the value of α/b is constrained by fitting a $2A > 0$ curve to laboratory slide-hold tests where $2A > 0$. The $2A = 11.5$ MPa data are used here because the theory predicts the greatest effect for the largest available $2A$. Unfortunately, the data on Figure 7 are highly scattered. The healing for the two 10-s holds is greater than that for the two 30-s holds. Paired measurements do not reproduce the same healing, especially for two 300-s and the two 1000-s holds. A hint that healing increases with hold time is defined by the 1000-s data along with the gross magnitude of the effect, but that is about all.

A value of $\alpha/b = 16$ gives a eyeball fit through the highly scattered data. An uncertainty estimate is obtained by noting that the theoretical difference between the $2A = 0$ and the $2A = 11.5$ MPa curves is increases with α/b. Increasing α/b by a factor of 2 gives a curve that passes through the highest values of the points (Figure 7).

The parameter α is also measured by normal traction stepping tests at constant velocity. Our values of $b = 0.0066$ and $\alpha/b = 16$ imply that $\alpha = 0.11$. This value of α is lower than the values obtained from normal traction stepping tests. *Richardson and Marone* [1999] obtained 0.3 on the samples discussed in this paper, and *Linker and Dieterich* [1992] obtained 0.2 on another suite of samples. Our value is not unreasonable as there was considerable uncertainty in these estimates and in our estimate.

3.3.4. Slip- and/or time-dependent behavior after holds. The time-dependent recovery of shear traction after restart following a hold is predicted by the theory to be an indication of the amount of strain rate delocalization. Longer holds and higher values of the normal traction oscillation $2A$ are predicted from the simple theory to delocalize strain rate upon restart. The preparation time is predicted to have a significant effect on behavior after brief holds for $2A = 0$.

We begin with the behavior after holds where $2A = 11.5$ MPa. The observed recovery curves for $2A = 11.5$ MPa are essentially linear (Figure 8). The model curves are linear for small times and have the slope observed in the laboratory experiments. Once about half the "healing" shear traction has recovered, the theoretical curves go quickly to zero.

The behavior of the theoretical curves can be understood as follows. Initially, the strain rate is distributed essentially uniformly across the gouge zone. Displacement of $W_{\text{nom}}\varepsilon_{\text{int}}$ is needed for the state variable to evolve and localization to begin.

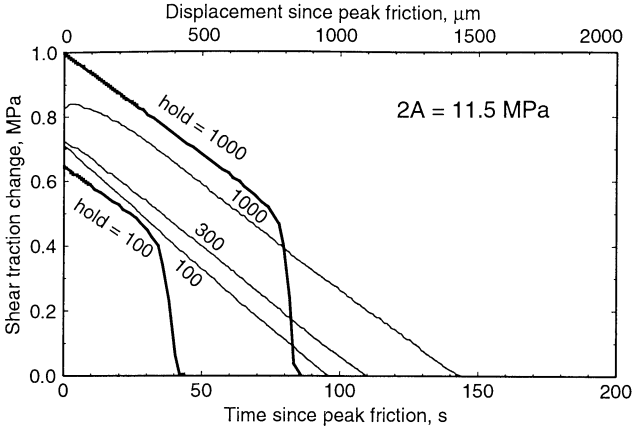

Figure 8. Recovery of shear traction following laboratory holds of 100, 300, and 1000 s shown by the light lines for $2A = 11.5$ MPa. The heavy lines show model results for 100 and 1000 s also with $2A = 11.5$ MPa. Time since peak friction and displacement since peak friction axes are given. The observed curves do not show the kink apparent in the theoretical curves. It is assumed for the numerical models that $h = 0.008 W_{\text{nom}}$ and that the preparation time is 384 s.

Once localization begins the width of the high-strain rate zone becomes W which is less than the full nominal width W_{nom}. The displacement to further localize strain rate $W\varepsilon_{\text{int}}$ decreases as the width W does. This causes rapid evolution to the steady state width W_{ss} of the high-strain rate zone and the steady state shear traction.

The linear form of the laboratory curves is not attributable to the fact that double-direct shear apparatus was used so that the observed shear traction is the sum of that on two gouge layers. In the real experiments the properties of the two zones probably differed, and the predicted rapid change in shear traction associated with localization is expected to have occurred at different times in each zone. From this reasoning, the measured shear traction curves are predicted to have separate kinks associated with each localization event if they are in fact the sum of two theoretical curves. However, the observed curves are linear without any kinks.

A more reasonable but qualitative explanation within the scope of the theory is that the observed linear behavior results because strain rate localization within the experimental gouge is a three-dimensional process rather than the one-dimensional one chosen for simplicity in the numerical simulations. We make no attempt here to formulate a three-dimensional theory of a fault gouge. Instead, we use the one-dimensional theory to obtain qualitatively differences its predictions and real three-dimensional strain rate localization.

First, our one-dimensional model presumes uniform material properties. One look at Figure 1 confirms the complex geometry of the real gouge. The particle size distribution and mean size differ significantly within and outside of the shear bands.

Returning to the absence of kinks in the observed curves in Figure 8, we suggest that the final strain rate localization occurred gradually rather than abruptly as in the theoretical curves. Gradual strain rate localization, but not necessarily a linear recovery curve, is expected in three-dimensional gouge where displacement in continuous. Heterogeneities in the

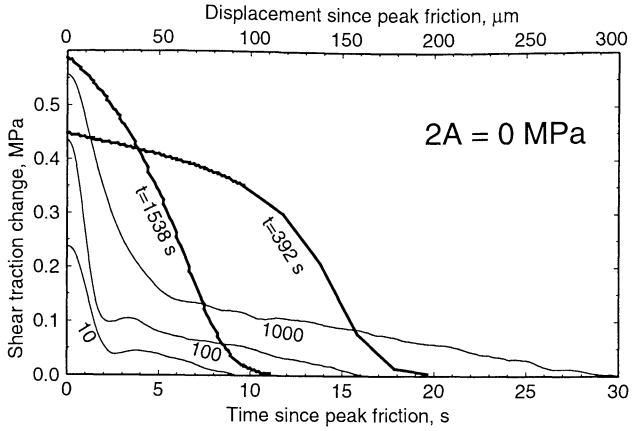

Figure 9. Observed recovery of shear traction following holds shown as in Figure 8. Theoretical results following a 100-s hold are shown for preparation times since last strain delocalization of $t=384$ s and 1538 s (heavy lines). The longer time fits the duration but not the shape of the observed curve (light line). It is assumed that $h=0.008W_{\text{nom}}$ in the numerical calculation.

gouge, as well as heterogeneities in the stress associated with them, tend to cause the strain rate to initially localize on different Y shears or B shears at various positions within the gouge zone. Riedel shears, which cannot be represented quantitatively in one dimension, may take up some of the strain. Time is required for a single Y shear or B shear to establish itself at the expense of the poorly aligned network of Y shears, B shears, and Riedel shears. In contrast, a single Y shear at the previous high-strain rate zone is established in the one-dimensional model as the vestiges of the high-strain zone prior to the hold are the only perturbation present.

The observed shear traction recovery for $2A = 0$ MPa provide another example which can qualitatively be attributed to three-dimensional deformation in the gouge. Observed recovery consists a rapid decrease in shear traction followed by a slower decrease (Figure 9). The observed time and displacement needed for recovery are much less than for $2A = 11.5$ MPa.

The model curves do not have the observed shape and are dependent on the preparation time since the last strain delocalization. The shape difference between the observed and laboratory curves is not an effect of elasticity. The results of a model including elasticity are shown in Figure 10. The slip-weakening curve with elasticity is similar to the very stiff case in Figure 9. That is, the predicted recovery of shear traction after the hold has the same duration but not the same shape and amplitude as observed.

The gross behavior of the slip-weakening $2A=0$ data is explained qualitatively within the scope of the theory in terms of three-dimensional effects in a limited part of the gouge zone. After a hold, most of the high-strain rate zone remains localized at is initial steady state width W_{ss} and a little is somewhat delocalized to a new width of W_{new}. During recovery the localized part recovers over a displacement of $W_{ss}\varepsilon_{\text{int}}$, and the partly delocalized part recovers over a displacement of $W_{\text{new}}\varepsilon_{\text{int}}$. The observed recovery curve may be interpreted has the sum of curves recovering over each length scale.

The effect of preparation time on strain rate delocalization upon restart is quantified in the models by the concept of strain rate amplification defined as the ratio of the maximum strain rate to a uniform strain rate over the nominal gouge width W_{nom} (Figure 11). From the theory, long preparation since the last strain rate delocalization affects the value of the state variable outside the zone of high strain rate. When this time is large, the state variable outside the high-strain zone is large, and the the ratio of the state variable outside the previous high-strain rate zone to the inside state variable does not change much dur-

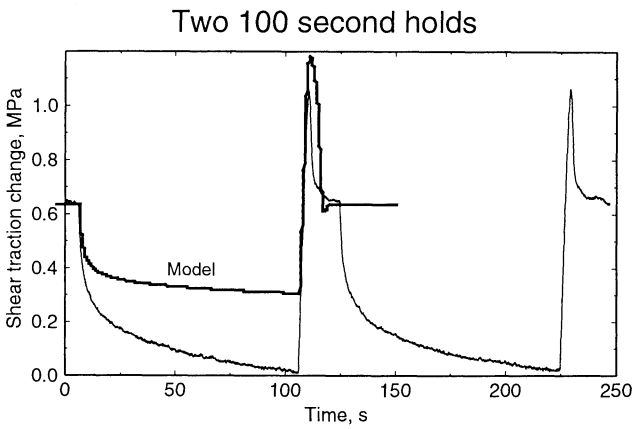

Figure 10. Observed shear traction during 100-s holds shown by the light line. The heavy line shows theoretical results for a spring slider model with the preparation time of 1538 s. The stiffness is 25 MPa mm^{-1}. It is assumed that $h=0.008W_{\text{nom}}$. The predicted relaxation of shear traction is somewhat less than observed. The duration but not the shape of the recovery curve is correctly predicted.

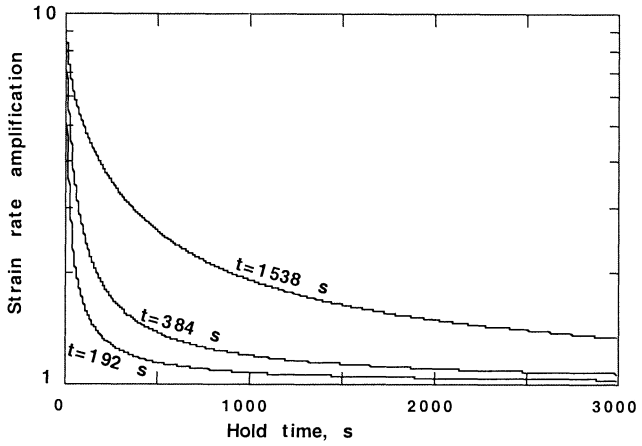

Figure 11. Computed strain rate amplification upon restart plotted as a function of hold time. The preparation time since the last strain delocalization is shown on each curve. Strain rate amplification is defined as the ratio of the strain rate at the fastest sliding grid point to the strain rate for uniform deformation in the gouge. That is, it is 1 when there is no strain rate localization. The continuum imposed by the length scale h makes these results nearly independent of the grid spacing. Localization upon restart decreases with hold time as the state variable becomes more uniform throughout the gouge as shown in Figure 4. The initial ratio of the state variable inside and outside the high strain zone increases with preparation time; longer holds are needed to reduce the ratio. The curves are computed using $h=0.016W_{\text{nom}}$ and $2A=0$.

ing short holds for $2A = 0$. For $2A = 0$ the predicted strain rate is already localized over most (but not all) of the area of the gouge zone upon restart. For example, most of the recovery for the observed 1000-s hold curve for $2A = 0$ in Figure 9 occurred within within a few seconds. In comparison, the observed recovery duration after the 10-s hold with $2A = 11.5$ MPa in Figure 8 (which has healing similar to the 1000-s hold curve in Figure 9) is ~100 s. In terms of the simple theory the brief preparation time of this experiment caused ψ_{out} to be small enough that essentially complete delocalization over all the area of the gouge zone occurred during the hold. The displacement to relocalize strain rate was $\sim W_{nom}\varepsilon_{int}$.

The relaxation of shear traction during the hold in the model is somewhat less than observed (Figure 10). This is consistent with results from *Marone* [1998] showing that relaxation is consistently underpredicted by a time-dependent state evolution law using constitutive parameters fit to small velocity step perturbations.

3.3.5. Dilatancy parameter. We obtain the intrinsic dilatancy factor obtained by curve fitting in Figure 5. Our preferred value of C_ε is about 3.4×10^{-3}, 20 times the apparent value determined by *Segall and Rice* [1995] from analysis of velocity stepping experiments. Our value derives from data taken after long hold times (≥1000 s) when the entire gouge zone was compacting. Our inferred shear strain rate localized to about 1/20 of the gouge zone width or more precisely the parameter h in dimensional units is between 17 and 34 μm. This compares with a grain size in shear bands of around 10 μm once the experiments were well underway. The critical strain ε_{int} for these values is 0.12 and 0.06, respectively. The ratio in (18) of dilatational strain to shear strain ($C_\varepsilon/\varepsilon_{int}$) is 0.028 and 0.056, respectively.

For comparison, the velocity-stepping experiments analyzed by *Segall and Rice* [1995] gave apparent values $\varepsilon_{app} = 0.005$ and $C_{app} = 1.7\times10^{-4}$. Their ratio of 0.037 is in good agreement with our theory, which predicts that this ratio is independent of strain rate localization. It is also in qualitative agreement with the prediction that these apparent values obtained by velocity stepping are less than the intrinsic values because of strain localization.

4. Discussion

We have discussed the implications of a unified theory for rate and state friction compiled by *Sleep* [1997]. This straightforward extension of rate and state friction to strain rate and state-dependent friction in a continuum allows strain rate localization to be studied. It is appropriate to compare its predictions with data. To do this, we have interpreted laboratory experiments in synthetic gouge by *Richardson and Marone* [1999].

The experiments of *Richardson and Marone*, 1999] which we analyze were not designed to consider strain rate localization. We can only indirectly study strain rate localization through its significant predicted effects on macroscopic properties. This being the case, doubt naturally arises as to whether strain rate localization is the correct explanation for the observed effects. Even if such doubts can be dismissed, one needs to know how well our theory represents observations. We address these issues in that order.

4.1. An Alternative Explanation to Strain Localization

A salient observation is that the observed displacement for recovery following holds where $2A > 0$ and long holds where $2A = 0$ was significant larger than the critical displacement observed for small velocity steps. In our theoretical interpretation, recovery occurs over a displacement scaling with $W_{new}\varepsilon_{int}$, where W_{new} is the effective width of the high-strain rate zone following a hold. Thus any process which delocalizes strain rate increasing W_{new} to greater than the steady state width W_{ss} is predicted to leave a long recovery displacement in its wake.

Alternative explanations for the process causing the long recovery time (or slip) are possible. M. Nakatani (personal communication, 1999) suggests consolidation strengthening of the gouge by vibrations. This phenomenon is well known in soil mechanics [*Lambe and Whitman*, 1969]. This familiar process explains settling of bulk products like cereal during transit. *Nakatani* [1998] attributed strengthening during holds where the shear traction was relaxed to this process.

We do not believe that consolidation strengthening is the explanation for the long recovery times observed by *Richardson and Marone* [1999]. In soils, consolidation strengthening occurs when the effective normal traction is essentially zero during part of the oscillation [*Lambe and Whitman*, 1969]. This situation should not have have arisen in the experiments of *Richardson and Marone* [1999]. For the nominal conditions of the $2A = 11.5$ MPa experiments the normal traction remained above 19 MPa compared to the mean value of 25 MPa. In the $2A = 5.6$ MPa experiments, normal traction nominally remained above 22 MPa.

In addition, consolidation strengthening in soils occurs when the initial packing is quite loose. It proceeds by rearrangement of grains rather than by internal deformation of grains. Although the porosity of the *Richardson and Marone* [1999] synthetic gouge is not precisely known, it is around 10%, which is far more dense than loose sands and soils with porosities of over 30%. The comminution of grains in their samples (Figure 1) indicates that deformation involved grain failure.

We note that disruption of strain rate localization might lead to long recovery times in situations other than slide-hold tests. For example, *Nakatani* [1998] reduced the shear traction on samples during holds and found that long recovery times result. *Sleep* [1999a] attributed the effect to variability of the normal traction on the gouge plane from its macroscopic value. At patches on low normal traction the movement of the blocks to reduce macroscopic shear traction locally reversed the sense of shear traction, causing slip of the opposite sense to the macroscopic slip. This reverse slip disrupted established shear bands, causing the sample to be stronger when slip resumed. Another possibility is that the reduction of shear traction caused unintended increases of normal traction on parts of the gouge contact which (as predicted by (21)) compacted and strengthened the gouge. These suggestions are plausible as the aftermath of strain localization was evident in the *Nakatani* [1998] samples.

In any case, experiments to distinguish the effects of consolidation strengthening from those predicted by our theory are possible. One possibility would be to vary the frequency of the normal traction variations (M. Nakatani, personal communication, 1999) . Consolidation strengthening is expected to be enhanced by high-frequency vibrations. In contrast, the healing during holds in our theory depends only on the integral I in (21) and is essentially independent of the frequency of the oscillations. In fact, the integral I depends mainly on the amount of time that the gouge is at the highest normal tractions encountered and is nearly independent of the history around low normal tractions. Various normal traction paths including ones where it remains above its previous value during the entire hold

can be conceived to give the same value of I and hence the same predicted recovery behavior at the end of the hold.

4.2. Appraisal of Theory Versus Observations

Our theory makes specific predictions about the behavior of macroscopic compaction and macroscopic shear traction during slide hold tests. Our one-dimensional formulation of the theory used in the numerical calculations gives only these macroscopic averages along with strain rate as a function of the distance x across the fault zone. This simplifying assumption makes the calculations tractable and avoids obscuring basic points with detail at the expense of not representing three-dimensional aspects of the gouge which are evident in Figure 1.

Unavoidable scatter occurs in the experimental results because the gouge is a complex substance and its intrinsic properties vary between tests. Avoidable scatter and systematic error also occurred because the history of the sample before each slide-hold test varied. In our numerical models we represented this history with a single parameter, the preparation time since strain rate was last delocalized.

We summarize how well our predictions match observations. The gross trend of compaction versus healing in Figures 5 and 6 is matched by the theoretical curves and the systematic difference of the $2A = 0$ data from the other data qualitatively explained by the longer effective preparation times of those slide-hold tests. A tolerable fit of healing versus hold time was obtained for $2A = 0$ in Figure 7. The $2A = 11.5$ MPa data in Figure 7 are quite scattered and detailed inferences from them are not possible.

The time-dependent behavior of recovery following holds provides a more stringent test of the theory because all available material parameters are already constrained by velocity-stepping tests and by analysis of Figures 5 and 7. In general, the observed duration of recovery (the time of the curves to approach zero) is correctly predicted in Figure 8 for $2A = 11.5$ MPa and in Figure 9 for $2A = 0$. The observed shape of the recovery curves is poorly predicted even when elasticity of the experimental apparatus is included in Figure 10.

We attribute the difference between the observed and theoretical recovery curves to three-dimensional effects in the synthetic gouge which we did not attempt to represent in the one-dimensional theory. That is, the strain rate delocalized by different effective widths W_{new} at different places within the plane of the gouge and relocalization of strain rate requires slip to organize into a single shear band. This process is potentially observable in real time as the local strain rate within the gouge could be measured while slip is occurring, say by X rays following marker grains. It is also modelable in that the evolution equation in (30) can be generalized to a convolution in two or three dimensions. That is, the gouge can be represented as a continuum fluid surrounded by boundary conditions for the sliding blocks. For the $2-\mu m$ numerical grid used in our models a huge calculation is implied which we are unable to do. The finite deformability of the blocks in the apparatus should also be included. Intrinsic unpredictability is implied by a three-dimensional instability for strain rate localization within a heterogeneous gouge.

4.3. Implications of Earthquake Rupture Modeling

One would like to include the results of laboratory experiments on synthetic gouge in models of earthquake dynamics. To do this, one needs to know how laboratory effects arise and whether they represent processes that can occur in the Earth. Empirical representations of laboratory results court the danger of including the same effect twice or omitting it altogether. As normal traction varies with time on real faults planes, it does not seem wise to have a separate formulation that works only in the case of constant normal traction. Thus we have analyzed constant normal traction data with variable normal traction data.

The theory of *Sleep* [1997] was compiled to be self-consistent and to have no unmeasurable parameters. It includes a relationship developed to explain transient changes in shear traction which occur in normal traction stepping experiments [*Linker and Dieterich*, 1992], here expressed in (5) and (1). This relationship has proven to be fairly robust. It can be easily extended to represent transient changes in friction following sudden changes in temperature as studied by *Chester* [1994, 1995] [*Sleep*, 1997]. It represents the shear failure strength of intact rock [*Sleep*, 1999b]. This may be a hint that it has a fundamental basis, although we make no claim that it is expressed in its optimal form.

In contrast, consolidation strengthening currently poses a problem to modeling the behavior of real faults. For example, the passage of a seismic wave is expected to strengthen a fault at rest as compaction is expected in the parts of the wave cycle when the shear traction and normal traction are reduced. A theory for this process needs to be formulated as a time-dependent evolution law to represent these changes. Alternatively, threshold values of vibration intensity for consolidation strengthening need to be defined. More experiments where the frequency and intensity of the normal and shear traction oscillations are varied are needed to do this in addition to appraising when and if consolidation strengthening occur in synthetic gouge.

The formulation for strain rate localization presented above may be useful to rupture dynamics. One cannot expect to model the properties of every part of the fault zone in great detail. Rather, macroscopic averages are relevant. For example, in the case of rupture where brief holds may lead to locking of a patch of the fault zone, the energy per area of fault zone needed to restart slip is relevant. Mathematically, this quantity is

$$Q = \int (\tau - \tau_{ss}) ds \quad , \tag{35}$$

where τ_{ss} is the shear traction for steady state sliding and s is displacement. This quantity is the area under the slip versus shear traction recovery curves in Figures 8 and 9. It can be seen that the theoretical curves have approximately the correct area within a factor of 2 of the observations. This result and the formulation in general do far better than ignoring strain localization altogether by using the short critical displacement obtained from velocity-stepping experiments as the recovery displacement.

5. Conclusions

We have modeled fault gouge has a continuum fluid using the unified theory rate and state friction complied by *Sleep* [1997]. The strain rate within the mathematical gouge localizes whenever $b > a$ The predicted "critical" displacement to significantly alter the strength of the gouge depends strongly on whether strain has localized or not. When the strain rate is essentially uniform throughout the macroscopic thickness of the gouge layer W_{nom}, the displacement is $W_{nom}\varepsilon_{int}$, where ε_{int} is the critical strain an intrinsic material parameter. When the strain

rate is localized to a steady state width W_{ss}, the displacement is $W_{ss}\varepsilon_{int}$. Partial delocalization to a width W_{new} is also possible. A one-dimensional continuum model of the gouge was formulated to make quantitative predictions of this behavior.

The results of slide-hold tests of *Richardson and Marone* [1999] were compared to the predictions of the theory. We found that the gross effects expected from strain rate localization occurred but could be studied only through their consequences on macroscopic variables. The analysis thus could not be divorced from the theory which predicts the macroscopic consequences from a continuum model. Firm evidence that strain rate localization actually occurred within the samples at the times predicted by the theory is lacking. Consolidation strengthening during normal traction oscillations is an alternative which cannot be excluded.

Overall, the theory gives a reasonable representation of the data. As expected, more healing and compaction of the fault gouge occurred when the normal traction was increased during the hold. Recovery times after holds were increased by the amounts expected from strain rate delocalization during holds. The one-dimensional theory, however, gave a poor representation of the shape of shear traction versus displacement curves during recovery. We attribute this qualitatively to the failure of the one-dimensional theory to represent the real complicated gouge.

A need to modify the previous experimental procedure became evident. The theory indicates that the history of strain delocalization before a particular slide hold test is important in determining its outcome. This preparation time since the strain rate was last delocalized is a simple conceptual way to represent this history. This quantity had not been previously recognized as significant in planning experiments. We recommend that the order of slide-hold tests be arranged so that the preparation time is kept more regular than was done in the *Richardson and Marone* [1999] experiments. As discussed above, the theory can be further tested as the behavior during holds is predicted to depend only on the integral of normal traction in (21). It would be nice but difficult to directly observe strain rate while slip is in progress.

Acknowledgments. We thank Masao Nakatani and an anonymous reviewer for useful suggestions and alternative explanations. This work was supported in part by the U.S. Geological Survey National Earthquake Hazards Reduction Program and in part by NSF grants EAR-9627895 and EAR-9805322.

References

Beeler, N. M., and T. E. Tullis, The roles of time and displacement in the velocity-dependent volumetric strain of fault zones, *J. Geophys. Res., 102*, 22,595-22,609, 1997.

Chester, F. M., Effects of temperature on friction: Constitutive equations and experiments with quartz gouge, *J. Geophys. Res., 99*, 7247-7261, 1994.

Chester, F. M., A rheological model for wet crust applied to strike-slip faulting, *J. Geophys. Res., 100*, 13,033-13,044, 1995.

Delaplace, A., G. Pijaudier-Cabot, and S. Roux, Progressive damage in discrete models and consequences on continuum modeling, *J. Mech. Solids, 44*, 99-136, 1996.

Dieterich, J. H., and B. D. Kilgore, Direct observation of frictional contacts: New insights for state dependent properties, *Pure Appl. Geophys., 143*, 283-302, 1994.

Gu, Y., and T.-f. Wong, Development of shear localization in simulated quartz gouge: Effect of cumulative slip and gouge particle size, *Pure Appl. Geophys., 143*, 387-423, 1994.

Lambe, T. W., and R. V. Whitman, *Soil Mechanics*, John Wiley, New York, 1969.

Linker, M. F., and J. H. Dieterich, Effects of variable normal stress on rock friction: Observations and constitutive equations, *J. Geophys. Res., 97*, 4923-4940, 1992.

Mair, K., and C. Marone, Friction of simulated fault gouge for a wide range of velocities and normal stress, *J. Geophys. Res., 104*, 28,899-28,914, 1999.

Marone, C., Effects of loading rate on frictional restrengthening: implications for fault healing and friction constitutive laws, *Eos Trans. AGU, 79*(17), S223, Spring Meet. Suppl., 1998.

Marone, C., and B. Kilgore, Scaling of the critical slip distance for seismic faulting with shear strain in fault zones, *Nature, 362*, 618-621, 1993.

Marone, C., and C. Scholz, Particle-size distribution and microstructures within simulated fault gouge, *J. Struct. Geol., 11*, 799-814, 1989.

Marone, C., C. B. Raleigh, and C. H. Scholz, Frictional behavior and constitutive modeling of simulated fault gouge, *J. Geophys. Res., 95*, 7007-7025, 1990.

Marone, C., B. E. Hobbs, and A. Ord, Coulomb constitutive laws for friction: Contrasts in frictional behavior for distribution and local shear, *Pure Appl. Geophys., 139*, 195-214, 1992.

Nakatani, M., A new mechanism of slip weakening and strength recovery of friction associated with mechanical consolidation of gouge, *J. Geophys. Res., 103*, 27,239-27,256, 1998.

Richardson, E., and C. Marone, Effects of normal force variations on frictional healing, *J. Geophys. Res., 104*, 28,859-28,878, 1999.

Scott, D. R., C. J. Marone, and C. G. Sammis, The apparent friction of granular fault gouge in sheared layers, *J. Geophys. Res., 99*, 7231-7246, 1994.

Segall, P., and J. R. Rice, Dilatancy, compaction, and slip instability of a fluid-infiltrated fault, *J. Geophys. Res., 100*, 22,155-22,171, 1995.

Sleep, N. H., Application of a unified rate and state friction theory to the mechanics of fault zones with strain localization, *J. Geophys. Res., 102*, 2875-2895, 1997.

Sleep, N. H., Rake dependent rate and state friction, *J. Geophys. Res., 103*, 7111-7119, 1998.

Sleep, N. H., Effects of the extrusion of fault gouge on frictional sliding, *J. Geophys. Res., 104*, 23,023-23,032, 1999a.

Sleep. N. H., Rate- and state-dependent friction of intact rock and gouge, *J. Geophys. Res., 104*, 17,847-17,855, 1999b.

C. Marone and E. Richardson, Department of Earth, Atmospheric and Planetary Sciences, Massachusetts Institute of Technology, Cambridge, MA 02139. (cjm@westerly.mit.edu; eliza@quake.mit.edu)

N. H. Sleep, Department of Geophysics, Stanford University, Stanford, CA 94305-2215. (norm@pangea.stanford.edu)

(Received July 8, 1999; revised June 9, 2000;
accepted July 24, 2000.)